

Comparison of sea-ice thickness measurements under summer and winter conditions in the Arctic using a small electromagnetic induction device

Christian Haas*, Sebastian Gerland[†],
Hajo Eicken*, and Heinz Miller*

ABSTRACT

Drillhole-determined sea-ice thickness was compared with values derived remotely using a portable small-offset loop-loop steady state electromagnetic (EM) induction device during expeditions to Fram Strait and the Siberian Arctic, under typical winter and summer conditions. Simple empirical transformation equations are derived to convert measured apparent conductivity into ice thickness. Despite the extreme seasonal differences in sea-ice properties as revealed by ice core analysis, the transformation equations vary little for winter and summer. Thus, the EM induction technique operated on the ice surface in the horizontal dipole mode yields accurate results within 5 to 10% of the drillhole determined thickness over level ice in both seasons.

The robustness of the induction method with respect to seasonal extremes is attributed to the low salinity of brine or meltwater filling the extensive pore space in summer. Thus, the average bulk ice conductivity for summer multiyear sea ice derived according to Archie's law amounts to 23 mS/m compared to 3 mS/m for winter conditions. These mean conductivities cause only minor differences in the EM response, as is shown by means of 1-D modeling.

However, under summer conditions the range of ice conductivities is wider. Along with the widespread occurrence of surface melt ponds and freshwater lenses underneath the ice, this causes greater scatter in the apparent conductivity/ice thickness relation. This can result in higher deviations between EM-derived and drillhole determined thicknesses in summer than in winter.

INTRODUCTION

The sea-ice thickness distribution in the polar regions has been shown to respond sensitively to global climate change (Mitchell et al., 1990). It is one of the key factors controlling the exchange of energy and momentum between atmosphere and ocean. Therefore, there has been much effort in the past to investigate and develop techniques to measure sea-ice thickness on regional scales. So far, apart from submarine sonar measurements of ice draft (e.g., Wadhams et al., 1992) the most promising technique for large-scale ice thickness determination seems to be airborne low-frequency electromagnetic (EM) induction (e.g., Kovacs et al., 1987; Kovacs and Holladay, 1990; Multala et al., 1995). In those studies, EM sounding systems were suspended below a helicopter or built into a fixed-wing aircraft, and measurements were performed in system heights of 15 to 20 m above the ice surface. The results indicated that

the thickness of level portions of sea ice can be estimated within 5% of drillhole determined ice thickness. In contrast, over deformed ice, e.g., in the vicinity of pressure ridges, results are not reliable. There, large deviations are a result of the variability within the footprint of the instruments, which is the area in which the secondary field is predominantly generated by induced currents and in which the ice thickness therefore is averaged. Kovacs et al. (1995) estimate the footprint size for vertical coaxial coil arrangements to be about 1.3 times the antenna height above the sea-ice/water interface, and 3.8 times for horizontal coplanar systems. Liu and Becker (1990) and Liu et al. (1991) numerically modeled the EM response over ice keels and developed algorithms to invert it into ice-keel shape, but these approaches are only of limited practical use because the structure of pressure ridges usually is too complex to be inverted realistically.

Manuscript received by the Editor June 19, 1995; revised manuscript received June 20, 1996.

*Alfred Wegener Institute for Polar and Marine Research, Columbusstrasse D-27568 Bremerhaven, Germany.

[†]Department of Geological Sciences, University College London, Gower Street, London WC1E 6BT, United Kingdom.

© 1997 Society of Exploration Geophysicists. All rights reserved.

Based on earlier work by Sinha (1976) and Hoekstra (1980), Kovacs and Morey (1991) performed ground-based measurements using a small portable steady-state induction device with coplanar coil arrangement to supplement airborne surveys. The instrument used was operated in the horizontal dipole mode and yielded reliable results within $\pm 10\%$ of the true ice thickness over level ice in the thickness range from 0.7 to 3.5 m, using only the quadrature component of the received secondary field. Compared with airborne measurements, this technique was easy to use, and the lateral resolution of thickness variations was 3 to 4 m, much better than for the airborne systems.

All the above studies were performed in the American sector of the Arctic and in the Baltic Sea, respectively, during winter and spring only. Because of its high resistivity, the ice is considered transparent for EM systems under these conditions. The conductivity of the seawater has to be assumed or is inverted from multifrequency soundings. Kovacs and Morey (1991) showed that small variations in ice and seawater conductivity do not alter the EM response significantly with respect to ice thickness inversion.

In this paper, we extend the application of EM sea-ice thickness measurements employing ground-based small-offset, loop-loop surveys to winter as well as summer conditions in different regions of the Arctic, using the technique of Kovacs and Morey (1991), and then compare them with drilling results. Based on ice-core analyses, conductivities of Arctic summer sea ice are determined. Then, by means of 1-D modeling of the EM response, it is examined to what extent the response is altered under summer conditions, when the ice is highly porous and contains a significant meltwater component. Particular attention is focused on special features occurring only in summer, such as surface melt ponds and meltwater lenses at the ice/water interface, because at least the former usually cover between 10 and 50% of the surface of Arctic summer sea ice (Maykut, 1986). Although ground-based measurements may not be adequate to measure ice-thickness distributions on regional scales, the findings from our applications of the EM method under summer conditions should be of great importance for the suitability of airborne surveys during the melt season as well.

STUDY AREAS

EM measurements were performed as part of sea-ice research programs conducted during a winter cruise and two summer cruises of the icebreaking research vessel *Polarstern*, which led to Fram Strait and to the Siberian Arctic, respectively (Figure 1).

The study area in the Laptev Sea is representative of ice conditions prevailing over the vast Eurasian shelves, from where first-year ice is exported into the Arctic Basin and after a period of a few years' transport in the Transpolar Drift is finally exported through Fram Strait. Thus, the areas studied represent the two "end-members" of Arctic sea ice, the thinner, young ice of the shelf seas and the aged, deformed multiyear ice in the ablation zone.

Conditions in winter (March 1993) were characterized by very low air temperatures (-40 to -33°C). Profiling was carried out on a snow-covered multiyear floe. The summer measurements (August–September 1993 and 1995) took place during warmer conditions always close below 0°C . Here, both

multiyear and first-year ice, lacking a snow cover and exhibiting extensive development of surface melt ponds, were investigated.

MEASUREMENTS

EM system

All EM measurements were performed with a standard Geonics EM31. This is a portable small-offset loop-loop steady-state induction device with a spacing r of 3.66 m between small transmitting and receiving coplanar antenna coils of 0.05 m diameter, forming good approximations of magnetic dipoles. The operating frequency f is 9.8 kHz. The instrument yields measurements of apparent conductivity σ_a , which is calibrated from the quadrature phase component of the ratio of the secondary and primary electromagnetic fields H_s and H_p as

$$\sigma_a = \frac{4}{\omega\mu_0 r^2} \text{Im} \left(\frac{H_s}{H_p} \right), \quad (1)$$

where ω is the angular frequency ($= 2\pi f$) and $\mu_0 = 4\pi \times 10^{-7}$ H/m is the magnetic permeability of free space. The indicated apparent conductivity is a measure of the integrated electrical conductivity of the half-space beneath the instrument.

The primary field generated by the transmitter coil induces eddy currents within the conductive subsurface. The resulting secondary EM field is measured, through compensation of the primary field, by the receiving coil. The magnitude of the secondary field is proportional to the distance between the coils and the subsurface and its conductivity (Keller and Frischknecht, 1966). In the case of sea ice with its low conductivity, the secondary field is induced mainly in the highly conductive ocean water. The salinity of Arctic seawater typically varies between 30 and 35‰ (e.g., Coachman and Aagaard, 1974), with temperatures between 0 and -1.8°C resulting in a conductivity between 2300 to 2900 mS/m (UNESCO, 1983).

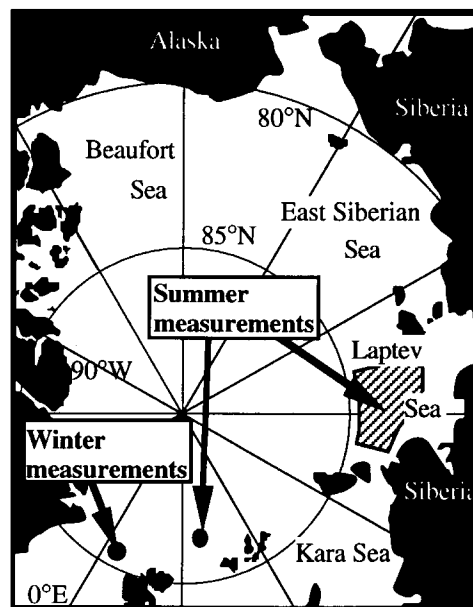


FIG. 1. Map of the Arctic Ocean showing the study regions in the Fram Strait and in the Laptev Sea.

Therefore, the strength of the secondary field is related directly to the distance between instrument and seawater, or to the sum of sea-ice thickness and (known) instrument height above the ice surface.

Field procedures

All profiles used a 4 m point spacing and were 100 to 250 m long (Table 1). At each point, the EM measurements were performed with the instrument placed directly on the snow/ice or melt pond surface and operating in the horizontal dipole mode, i.e., the coil planes were aligned vertically. This mode yields the most accurate interpretations (Kovacs and Morey, 1991) that is mainly a result of the smaller footprint size compared with measurements in the vertical dipole mode (Kovacs et al., 1995; see also in the Introduction).

In addition to the along-profile measurements, a number of individual surface melt ponds were cross-profiled with point spacings varying from 1 to 5 m. Melt ponds typically are some meters to a few tens of meters in diameter and 0.2 to 0.4 m deep.

Direct measurements of snow depth, ice thickness, and freeboard were conducted in holes drilled at 4 m spacing. In addition, one or several ice cores were taken along each profile for temperature measurements and analysis of ice microstructure and physical properties including ice conductivity (for details of ice-core analysis, see Eicken et al., 1995).

In total, EM and direct measurements were performed at roughly 400 single points along 12 standard profiles during both expeditions and additional melt-pond cross-profiles.

1-D modeling

To examine the influence of different conductivities of winter and summer sea ice as derived by the ice-core analyses on the electromagnetically measured apparent conductivity, 1-D modeling of the EM response (quadrature component of the relative secondary field) to changing total ice thickness and changing ice conductivity was performed. Full solution formulas for this are given, e.g., by Ward and Hohmann (1988)

Table 1. Mean EM and drillhole derived ice thickness \bar{z}_{iEM} , \bar{z}_{iDrill} and their standard deviations s and the deviation $\delta = (\bar{z}_{iEM} - \bar{z}_{iDrill})/\bar{z}_{iDrill} \times 100$ for each single profile.

Profile	Length (m)	\bar{z}_{iEM} (m)	s_{EM}	\bar{z}_{iDrill} (m)	s_{Drill}	δ (%)
W1	204	2.85	0.66	2.81	0.59	1.4
S1	122	3.25	1.17	3.05	1.08	6.6
S2	100	0.74	0.26	0.78	0.28	-5.1
S3	100	1.66	0.63	1.65	0.71	0.6
S4	100	1.79	0.42	1.80	0.60	-0.6
S5	100	1.83	0.27	1.84	0.37	-0.5
S6	48	1.74	0.06	1.70	0.04	2.4
S7	100	1.85	0.30	1.89	0.32	-2.1
S8	100	2.38	0.36	2.37	0.45	0.4
S9	100	1.95	0.55	1.96	0.51	-0.5
S10	122	2.56	1.30	2.37	1.07	8.0
S11	100	2.97	0.66	3.12	0.60	-4.8
All (Summer)	1092	2.07	0.93	2.08	0.91	-0.5

and were programmed using a digital filter method (Anderson, 1979). For the modeling, we assumed a seawater conductivity of 2600 mS/m being a mean surface-water value measured by CTD casts onboard *RV Polarstern* during the summer cruises (Schauer, pers. comm.) and a coil height of 0.14 m above the snow/ice surface.

RESULTS

Conductivity-thickness transformation

As a data example, in Figure 2 an apparent conductivity profile is compared with drillhole determined ice thickness (in the following, total ice thickness, i.e., ice and snow thickness, is referred to as ice thickness) along the same profile. A strong negative correlation between apparent conductivity and ice thickness is obvious.

Plotting apparent conductivity versus ice thickness for all individual measurements establishes a strong negative exponential relationship (Figure 3). By fitting exponential functions to these data, transformation equations are obtained for the conversion of apparent conductivity σ_a (mS/m) to ice thickness z_i (m). Different transformation formulas were obtained for the winter and summer data sets (Figure 3).

The fits

$$\sigma_{aw} = 95.8 + 1095.5 \exp(-0.995z_{iw}) \quad (2a)$$

and

$$\sigma_{as} = 57.2 + 1270.9 \exp(-0.900z_{is}), \quad (2b)$$

where indices w and s indicate winter and summer data, respectively, explain 91% (winter) and 98% (summer) of the total variance in the data. An estimate of the relative variance s^2 of the measurements can be gathered by means of Chi-square statistics, since χ^2 resulting from the fit should be approximately equal to 1 per degree of freedom. Based on $s^2 = 9.7\%$ for the winter and $s^2 = 13.8\%$ for the summer data, χ^2 of 1.03 and 0.99 per degree of freedom result, respectively, indicating an appropriate estimate of variances. From these, no

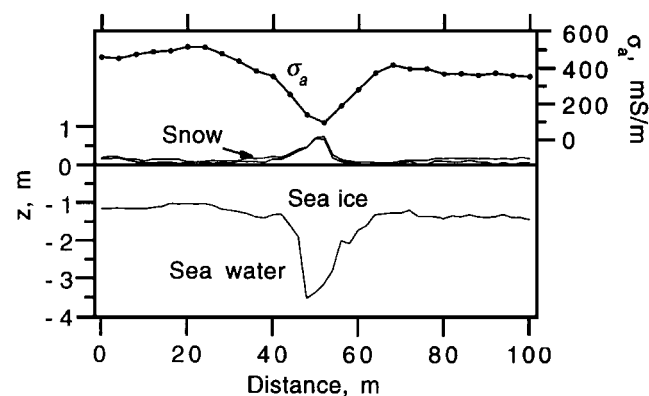


FIG. 2. 100 m long profiles of snow and ice thickness and apparent conductivity σ_a as measured in the horizontal dipole mode with the instrument placed on the ice surface (summer, profile S3). The zero line on the left axis marks the sea level. Spacing of drillholes is 2 m; that of EM measurements is 4 m.

significant difference between the winter and summer data can be deduced. Pooled winter and summer data result in

$$\sigma_a = 62.5 + 1273.9 \exp(-0.915z_i), \quad (2c)$$

explaining 98% of the total variance, s^2 being 13.6% ($\chi^2 = 0.99$).

Inversion of equations (2a), (2b), and (2c) yields the transformation equations

$$z_{iw} = 7.03 - \ln(\sigma_{aw} - 95.8)/0.995, \quad (3a)$$

$$z_{is} = 7.94 - \ln(\sigma_{as} - 57.2)/0.900, \quad (3b)$$

and

$$z_i = 7.81 - \ln(\sigma_a - 62.5)/0.915. \quad (3c)$$

An application of the transformation equation (3b) is presented in Figure 4a, showing the EM-derived and drillhole determined ice thickness for the profile of Figure 2. In Figure 4b, the deviation

$$\delta z_i = (z_{iEM} - z_{i\text{drill}})/z_{i\text{drill}} \times 100 \quad (4)$$

of the EM-derived thickness z_{iEM} relative to the drilling results $z_{i\text{drill}}$ is presented.

On all profiles, EM-derived and drillhole determined thicknesses match well for winter and summer data. In most cases, the deviations are less than $\pm 10\%$. On level ice, characterized by small lateral thickness variations (0–40 m and 75–100 m in Figure 2), the accuracy is even better and the deviations seldom exceed $\pm 5\%$. Thus, over level ice no significant difference occurs between measurements performed in winter and in summer.

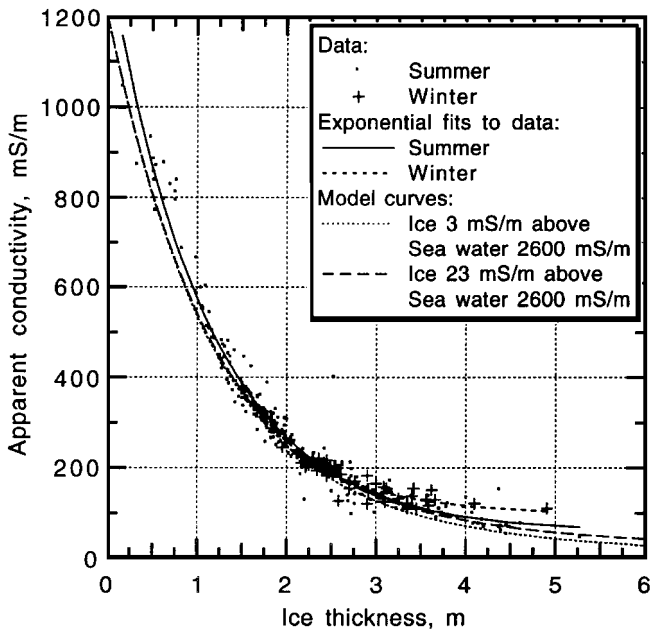


FIG. 3. Measured apparent conductivity versus ice thickness for the complete winter and summer data sets and the exponential fits according to equations (2a) and (2b) for winter and summer data. Also plotted are two two-layer 1-D model curves for ice floating on water with a conductivity of 2600 mS/m. Ice conductivities of 3 and 23 mS/m (see text) have been assumed.

As also found in all other studies referred to in the Introduction, EM-derived thicknesses differ significantly from drillhole determined thickness only in ridged areas. There, deviations can be as high as 40%.

Melt-pond cross-profiles

Figure 5 presents ice surface and draft profiles determined by drilling across three melt ponds. Also, the EM-derived draft is shown as calculated by means of equation (3b) and by subtraction of the ice freeboard which is zero over melt ponds. While EM and drilling results agree well in Figure 5a, the true draft is underestimated in Figure 5b, whereas it is overestimated in Figure 5c. The pond-water salinity of the ponds shown in Figures 5a and 5c was close to zero, but the water of the pond in Figure 5b had a salinity of 17.2%, with a temperature of -1°C resulting in a conductivity of 1473 mS/m. Therefore, the measured apparent conductivity was too high, resulting in an ice-thickness estimate too small compared with the true thickness. In Figure 6, the apparent conductivity from all measurements over melt ponds is plotted versus drillhole determined ice plus melt-water thickness. As in Figure 3, a negative exponential relationship can be seen. Also included in Figure 6 is a model curve for a 2-layer model with a water conductivity of 2600 mS/m and an ice conductivity of 23 mS/m resulting from the ice-core analyses below (see also Figure 3). This curve explains 84% of the total variation of the melt-pond data, thus indicating a greater scatter of measurements performed over melt ponds than over pond-free ice. Still, in most cases satisfactory ice plus meltwater thickness values could be derived.

Ice-core analyses

To yield an estimate of the bulk electric ice conductivity of winter and summer sea ice as input parameters for the 1-D

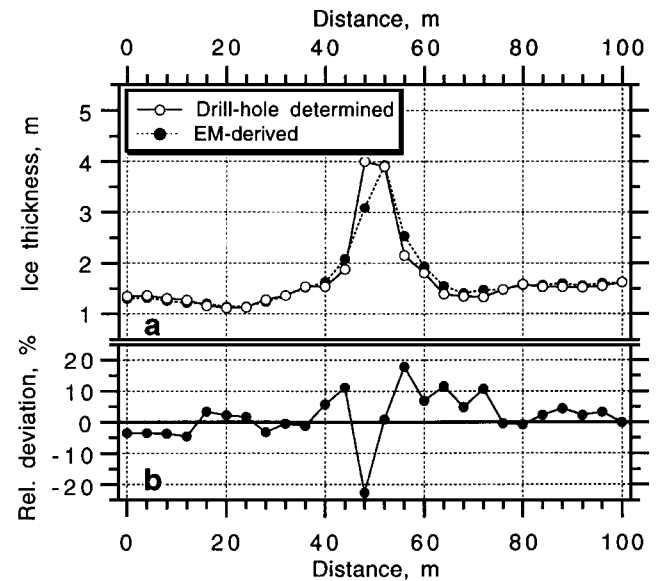


FIG. 4. (a) Ice thickness z_i determined from drillholes and by means of equation (3a) along the profile of Figure 2. (b) Deviation $(z_{iEM} - z_{i\text{drill}})/z_{i\text{drill}} \times 100$ between drillhole determined and EM-derived ice thickness in Figure 4a.

modeling, ice cores were analyzed for values of brine volume. The stratigraphy, microstructure, and salinity profiles of all cores were typical for Arctic multiyear ice (Eicken et al., 1995).

For the estimation of relative brine volume, fourth-degree polynomials were fitted to the measured temperatures of the winter cores, and linear temperature profiles from 0°C at the top to melting temperatures (-1.8°C) near the bottom of the ice were assumed for the summer ice cores, consistent with field measurements. Relative brine volumes V_b/V were calculated according to Cox and Weeks (1983):

$$\frac{V_b}{V} = \frac{\rho S}{F_1(T)}, \quad (5)$$

where ρ and S are the bulk density and salinity of an ice sample and F_1 is a coefficient dependent on temperature T . For temperatures above -2°C , $F_1(T)$ was taken from Leppäranta and Manninen (1988). Gas volume was assumed to be 10%. In Figure 7, two typical temperature and brine volume profiles are presented for sea-ice cores taken in winter and summer. Because of the very low ice temperatures (Figure 7a), brine volumes are very small in winter compared to summer (solid and open symbols, respectively in Figure 7b). Mean brine volume of all cores drilled in winter was 13.6%, and 93.4% of all

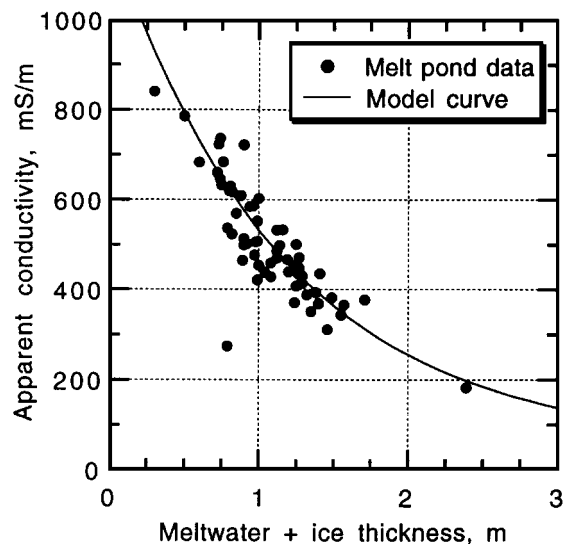


FIG. 6. Apparent conductivity as measured in horizontal dipole mode with the instrument placed immediately above the surface of melt ponds versus meltwater plus ice thickness. The solid line is a 1-D model curve for salinities of 23 and 2600 mS/m for ice and sea water, respectively (cf., Figure 3).

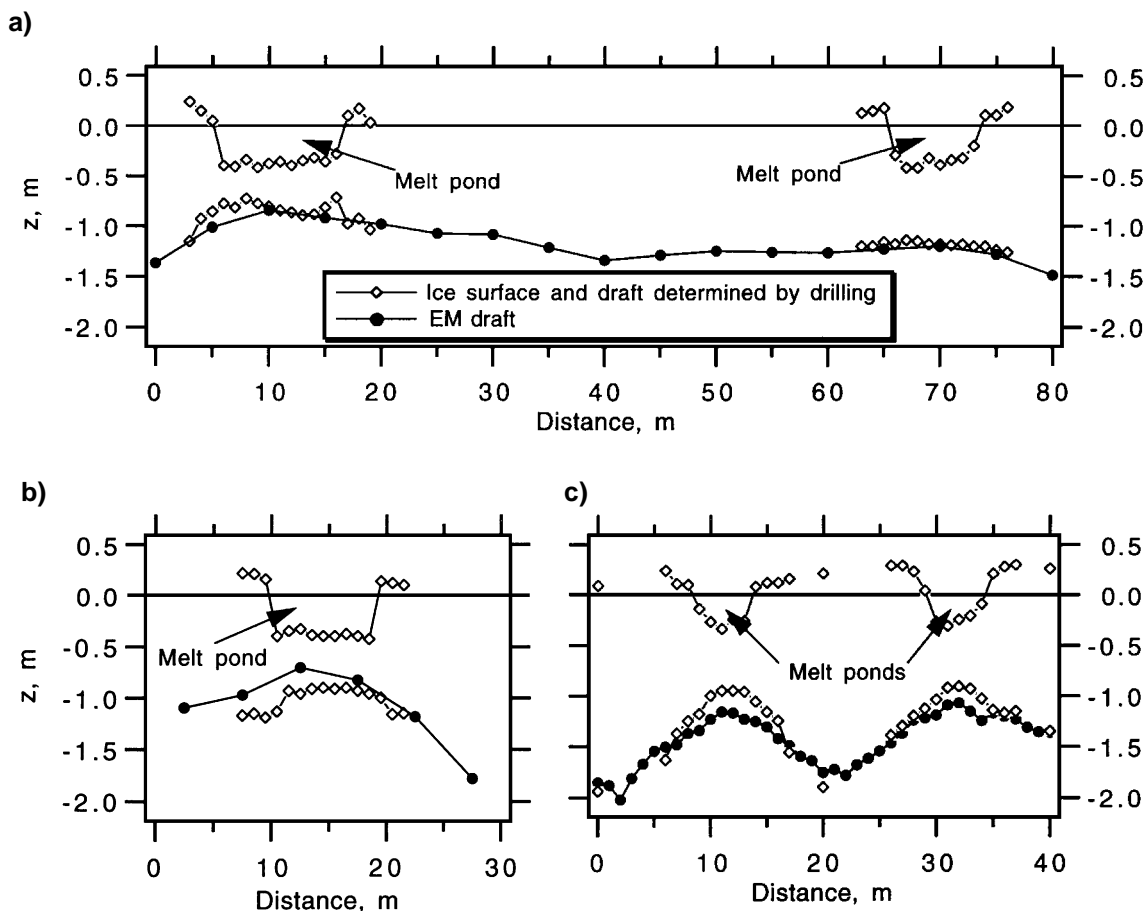


FIG. 5. Melt pond cross-profiles as determined by drillhole and EM measurements. The EM draft was calculated by means of equation (3a) and subtraction of ice freeboard which is zero over melt ponds because the pond surface is at sea level ($z = 0$).

summer cores, the latter value being slightly smaller than mean brine volumes of summer multiyear ice in the Eurasian sector of the Arctic Ocean found in Eicken et al. (1995), which ranged from 100 to 150%.

To calculate bulk ice conductivities from the measured temperatures and brine volumes, we followed a procedure suggested in Morey et al. (1984) and Kovacs and Morey (1988). It takes into account that sea ice is a mixture of pure ice and brine. While the pure ice fraction is considered to be nonconducting, the temperature-dependent conductivity σ_b of the brine is given by (Stogryn and Desargant, 1985)

$$\sigma_b = -T \exp(0.5193 + 0.08755T); \quad T \geq -22.9^\circ\text{C}$$

and

$$\sigma_b = -T \exp(1.0334 + 0.11T); \quad T < -22.9^\circ\text{C}. \quad (6)$$

A relationship between the conductivity σ_i of brine-saturated media and their porosity Φ is given by the empirical Archie's law (Archie, 1942)

$$\sigma_i = \sigma_b \Phi^m, \quad (7)$$

where m is an empirical constant ("cementation factor"). Originally, this expression was derived for permeable sandstones displaying no preferred shape or orientation of pores. For m , Morey et al. (1984) derived values between 1.55 in the top and 1.75 near the bottom of the ice, while Thyssen et al. (1974) found a value of 2.2. In our calculations, we choose $m = 1.75$.

Sea-ice conduction is believed to occur mainly in vertically aligned brine channels and the porosity is smaller than in most sandstones. However, since a comprehensive theory of conduction processes in sea ice is highly involved, Archie's law provides a first estimate of sea-ice conductivity.

Conductivity profiles were calculated for all cores as outlined above. This resulted in a mean ice conductivity of 3 mS/m for

the winter cores and 23 mS/m for the summer cores, respectively.

The results of the 1-D modeling using these two values as conductivities for the ice are also included in Figure 3. As in the measurements, apparent conductivity decreases exponentially with increasing ice thickness. The effect of the different ice conductivities is rather small, getting larger with increasing ice thickness, as more and more ice is contained in the region sensed by the instrument. Both curves provide a sufficient fit to the data at small and intermediate ice thicknesses.

DISCUSSION

Validity of transformation equations

Equations (3a), (3b), and (3c) are empirical relations, which implies that they are only valid for conditions similar to those for which the underlying data set was obtained. However, the ice-core results demonstrate that the state of the ice cover during both surveys was representative of Arctic multiyear pack ice during seasonal extremes. Hence, equation (3a) may be used for most Arctic multiyear ice at very low temperatures, while equation (3b) is valid for Arctic multiyear ice in summer, or equation (3c) could be used for all data. Furthermore, the transformations are only valid within certain thickness limits. Strictly, they can only be used for the thickness and conductivity range covered by the underlying data set. Further data are required for larger thicknesses, although here the problem of the 3-D nature of the measurements enters, because larger thicknesses are most likely to occur in deep draft pressure ridges.

Another estimate for the range in which reliable measurements could be performed is provided by the slope of the curves in Figure 3 and equations (2), respectively, since they reflect the dynamic response of the instrument with respect to ice thickness variations. Thus, to resolve a change in thickness of 0.1 m, the gradient of the curves should be larger than 2 mS/m per 0.1 m thickness variation, if the instrument reading is taken to be stable within ± 2 mS/m (which from our experience is a reasonable assumption). This is achieved for thicknesses less than about 4 m and 4.5 m for the winter and summer data, respectively, and for less than 5 m for the 1-D model curves. For comparison, the theoretical 1-D sensitivity of measurements carried out in the vertical dipole mode is slightly better, being sufficient for thicknesses of up to 5.6 m (curves not shown here). To extend the thickness range of EM measurements, an instrument with a better signal-to-noise ratio or a wider coil spacing has to be used, although this would reduce the lateral resolution.

It should be noted that equations (3) were derived from real data gathered over both level as well as thicker deformed ice (see also below), even though the method was shown to be less reliable over the latter. If it were surely known in advance that the ice was level and undisturbed, then a transformation equation could have been used derived by inversion of a fit to a 1-D model curve. For example, fitting an exponential function to the 23 mS/m curve in Figure 3 in the 0 to 5 m thickness range would yield a transformation equation

$$z_i = 8.38 - \ln(\sigma_a - 43.3)/0.842 \quad (8)$$

($r = 1.0$) which would result in the most accurate thickness interpretations of level ice, much better than by use of

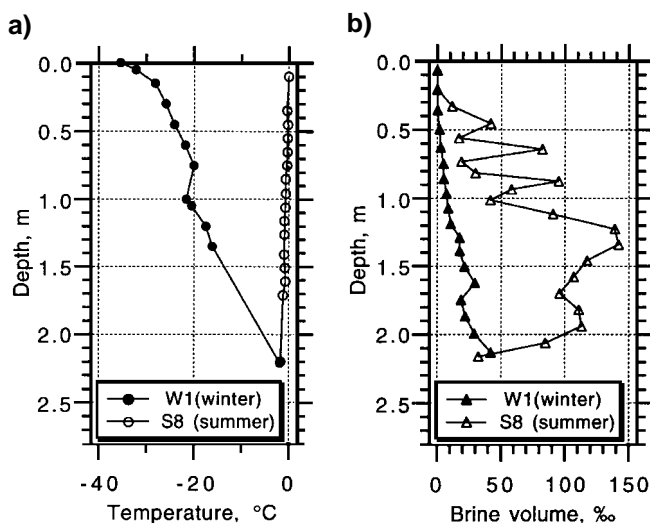


FIG. 7. Temperature (a) and brine volume (b) profiles of two typical multiyear ice cores obtained during ARK-IX/1a (from profile W1, solid symbols) and ARK-IX/4 (from profile S8, open symbols).

equation (3). But the problem is that in many cases the ice cannot be assumed to be level and undeformed in advance, equations (3) thus being better choices for the general case of measurements in the field.

This discussion shows that from a different point of view, the problem of accuracy of the EM measurements can be considered as the problem of identifying whether a stretch of sea ice is level or deviates from an ideal one-layer case. To meet this problem fully, a multifrequency instrument would be needed, allowing to reduce the ambiguities inherent to the use of a single-frequency instrument only.

Comparison of EM-derived and drillhole determined thickness

Table 1 lists mean EM-derived and drillhole determined thicknesses \bar{z}_{iEM} and $\bar{z}_{i\text{drill}}$ for all 12 profiles along with their standard deviations s_{EM} and s_{drill} . Additionally, the deviations between the means \bar{z}_{iEM} and $\bar{z}_{i\text{drill}}$ are presented. Although measurements at individual points in the region of pressure ridges can deviate largely, these deviations almost seem to vanish if mean values for complete profiles and in particular across pressure ridges are considered. Apparently, the positive deviations at ridge flanks effectively compensate the negative deviations over ridge crests (Figure 4). Still, the largest deviations occur for profiles S1 and S10, which also exhibit the largest standard deviations, corresponding to a rough thickness profile. Further, s_{EM} is strongly correlated with s_{drill} ($r = 0.97$, Table 1), showing that EM profiles across rough ice do not generally appear smoothed. This is also a result of thickness variations perpendicular to the profile direction that are not at all represented in the drilling data.

The problems encountered in deformed ice are also reflected in the deviations between model curves and the exponential fits to the data at ice thicknesses bigger than 3 to 4 m in Figure 3. Since the model curves have been calculated with a 1-D model, they give the expected apparent conductivity at a certain thickness of a level, infinitely extended plate of ice. In contrast, the data presented in Figure 3 have been measured on both level and deformed ice, the larger thicknesses almost entirely caused by measurements over pressure ridges. Here, as a result of the areal averaging of the subsurface conductivity, the determined apparent conductivity is higher than in the case of level ice of the same thickness.

Measurements on summer sea ice

The extreme differences in general physical properties of winter and summer sea ice are only of minor importance for ice conductivity, introducing little difference between winter and summer data and the model curves in Figure 3. Still, although this difference is not significant, the apparent conductivities over ice of intermediate thickness (1 to 2.5 m) measured in winter are smaller than in summer, indicating lower ice conductivities. The model results emphasize that at both seasonal extremes EM measurements are a suitable tool to determine ice thickness. That this is also true for measurements in summer is because of the properties of the meltwater. Although brine volumes of summer sea ice are much higher than in winter, the brine and meltwater filling the pores have only low salinities, because brine and ice generally are in a phase equilibrium, and warm ice cannot coexist with high salinity brine. For example,

average brine salinities of typical multiyear ice in summer as directly measured by Eicken et al. (1995) range from 4.8‰ in the top to 16.7‰ in the lower parts of the ice column, i.e., are much smaller than seawater salinity. Thus, the resulting ice conductivity of 23 mS/m derived here is only slightly greater than the 3 mS/m for the winter ice, making the summer ice transparent for the EM dipole fields. Since the conductivity contrast between the ice and seawater remains very large, the EM measurements are not altered significantly.

The seasonal differences between physical properties of the ice are mainly caused by different ice temperatures at the respective time of the year. To investigate the effect of temperature on the electrical conductivity profile within Arctic multiyear ice with a typical mean salinity profile [calculated from 66 cores by Eicken et al. (1995)], we calculated ice conductivity profiles for surface temperatures of 0, -1.8 , -10 , -20 , -30 , and -40°C , assuming a linear temperature profile from the top to the bottom, the latter taken to be at the melting temperature of -1.8°C (Figure 8a). The complete range of seasonal extremes is covered by these values. Ice conductivities for each depth interval (0.01 m resolution) were calculated as described above (Figure 8c). Since the bottom temperature is the same for all profiles, differences mainly occur in the middle and top portions of the profiles. Ice conductivities are highest for the 0°C -surface-temperature profile and lowest for the -40°C profile. It is important to note that the largest differences occur between the 0 and -1.8°C profiles, while below surface temperatures of -10°C ice conductivity does not vary much. Thus, ice properties relevant for the EM measurements vary little throughout most seasons and change only significantly during summer. Still, as outlined above, the EM measurements are hardly affected in any season. Apart from brine volume, brine conductivity also enters into the calculation of ice conductivity according to equation (7). Brine conductivity profiles for the respective surface temperatures calculated from equations (6) are plotted in Figure 8b. Generally, as brine temperature decreases, brine salinity increases. This leads to increasing brine conductivity only down to a temperature of -11.4°C . Below this temperature, ion mobility in the brine is reduced and therefore its conductivity decreases with temperature. For ice conductivity this implies that decreasing brine volume due to decreasing temperature is compensated by increasing brine conductivity, but only down to -11.4°C . Below this temperature, both brine volume and brine conductivity cause reduced ice conductivity.

Similar to the ice, in most cases melt ponds were found to be transparent for the EM fields, since their water is derived from the melting of snow and low-salinity upper ice layers (Figure 7). For example, water samples obtained from a larger number of surface melt ponds by Eicken et al. (1994) had a mean salinity of 2.9‰, with a broad maximum of the distribution at about 0.5 to 1‰, resulting in very small conductivities. Therefore, the total thickness of the ice plus meltwater layer is correctly determined. Nevertheless, the melt-pond measurements show a larger scatter than measurements over pond-free ice (Figures 3 and 6). This, on the one hand, is caused by the fact that melt ponds may in some cases exhibit higher salinities approaching those of seawater (Eicken et al., 1994). On the other hand, the scatter of the pond data is more likely due to the fact that the ice bottom topography below ponds often is vaulted upward (like in the extreme example in Figure 5c), as a result of enhanced

melting caused by higher energy absorption within the low-albedo ponds. These morphological features affect measurements in the same way as ridges do.

Other common features occurring in summer are melt-water lenses or under-ice melt ponds forming underneath the ice as a result of meltwater runoff at floe edges or downward percolation of meltwater (Wadhams and Martin, 1990; Eicken, 1994). Typically, the thickness of these lenses ranges from a few centimeters to a few decimeters. Because the density of meltwater is lower than that of the seawater, it tends to collect at the ice bottom, in particular within depressions such as are often found beneath surface melt ponds. Since the meltwater is highly transparent to the EM fields, ice thickness is overestimated in such cases (as may be the case in Figure 5c). However, since much of the meltwater entrapped underneath the ice freezes due to the contact with the cold seawater even during summer (Eicken, 1994), this meltwater could still be considered as part of the ice cover, being only temporarily in a fluid phase. The problem with under-ice meltwater lenses is that their presence generally cannot be predicted.

CONCLUSIONS

The results shown demonstrate that the small-offset loop-loop EM technique can be applied successfully for the indirect determination of level sea-ice thickness, extending the previous work conducted in the North American Arctic under winter and spring conditions (Kovacs and Holladay, 1990; Kovacs and Morey, 1991) to the Eurasian Arctic and to the summer season. Comparison of winter and summer data bracketing the most extreme conditions to be encountered during measurement campaigns in conjunction with ice-core studies demonstrated the robustness and general applicability of the technique.

Melt season conditions with their fundamental differences in physical sea-ice properties introduce greater scatter into the ice-thickness versus apparent conductivity relation, because ice conductivity can vary in greater ranges than in winter. Surface melt ponds typical for Arctic summer sea ice are almost transparent for the EM fields and allow ice plus meltwater thickness to be determined correctly in most cases. Under-ice melt ponds, where they exist, generally result in overestimates of ice thickness of some centimeters to one or two decimeters. This could be a concern for engineering applications of ice-thickness measurements.

The study showed that for level and moderately deformed ice, empirical conductivity-thickness relations may provide reliable, readily available ice-thickness estimates. Moreover, the study showed that these relations also hold for summer sea ice even in areas of melt ponds.

Although for greater ice thicknesses observed in pressure ridges the accuracy of the EM-derived thickness decreases significantly and may be rather poor, the technique does at least provide valuable data on the distribution and typical length scale of such thick or deformed ice. These are important variables for the validation of sea-ice models (Harder and Lemke, 1994).

Measurements presented here, like those of Kovacs and Morey (1991), were performed with a portable small-offset loop-loop instrument. Operated during station times of ice-breaking research vessels cruising through ice-covered regions, these measurements can yield representative data on the regional thickness distribution. Furthermore, the results of this study with respect to measurements over summer sea ice also apply to airborne EM surveys, which can operate much more effectively.

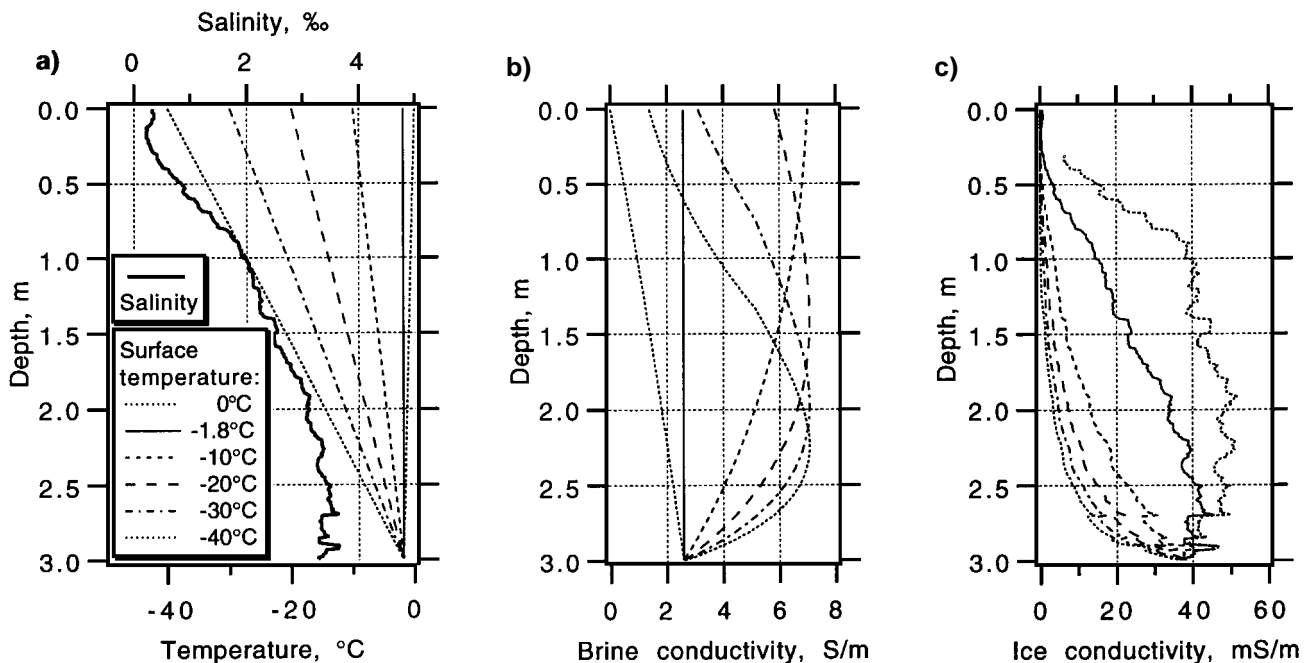


FIG. 8. Profiles of mean salinity (a; top axis, thick line; see text) and different temperatures (a; bottom axis, thin lines) used as input for the calculation of profiles of electrical brine (b; only dependent on temperature) and ice conductivity (c). The air-temperature legend of (a) is also valid for the curves in (b) and (c).

ACKNOWLEDGMENTS

S. Hanke, R. Pac, E. Reimnitz, D. N. Thomas, and F. Valero are gratefully acknowledged for indefatigably drilling holes into the ice. Without the support of captain and crew of *RV Polarstern* it would not have been possible to obtain the data for this paper. Suggestions by S. Arcone considerably improved the manuscript. This is AWI publication no. 919.

REFERENCES

- Anderson, W. L., 1979, Computer Program. Numerical integration of related Hankel transforms of orders 0 and 1 by adaptive digital filtering: *Geophysics*, **44**, 1287–1305.
- Archie, G. E., 1942, The electrical resistivity log as an aid in determining some reservoir characteristics: *Trans., Am. Inst. Min., Metall., Petr. Eng.*, **146**, 54–62.
- Coachman, L. K., and Aagaard, K., 1974, Physical oceanography of Arctic and subarctic seas, in Herman, Y., Ed., *Marine Geology and Oceanography of the Arctic seas*: Springer-Verlag, 1–72.
- Cox, G. F. N., and Weeks, W. F., 1983, Equations for determining the gas and brine volumes in sea-ice samples: *J. Glaciol.*, **29**, 306–316.
- Eicken, H., 1994, Structure of under-ice melt ponds in the central Arctic and their effect on the sea ice cover: *Limnol. Oceanogr.*, **39**, 682–694.
- Eicken, H., Alexandrov, V., Gradinger, R., Ilyin, G., Ivanov, B., Luchetta, A., Martin, T., Olsson, K., Reimnitz, E., Pac, R., Poniz, P., and Weissenberger, J., 1994, Distribution, structure and hydrography of surface melt puddles, in Fütterer, D. K., Ed., *The expedition ARCTIC '93, leg ARK-IX/4 of RV "Polarstern" in 1993: Reports on Polar Research*, **149**, 73–76.
- Eicken, H., Lensu, M., Leppäranta, M., Tucker III, W. B., Gow, A. J., and Salmela, O., 1995, Thickness, structure and properties of level summer multi-year ice in the Eurasian Sector of the Arctic Ocean: *J. Geophys. Res.*, **100**, 22,697–22,710.
- Harder, M., and Lemke, P., 1994, Modelling the extent of sea ice ridging in the Weddell Sea, in Johannessen, O. M., Muench, R. D., and Overland, J. E., Eds., *The polar oceans and their role in shaping the global environment*: Am. Geophys. Union, *Geophys. Mono.* **85**, 187–197.
- Hoekstra, P., 1980, Theoretical and experimental results of measurements with horizontal magnetic dipoles over sea water to measure ice thickness and water salinity: *Geo-Physi-Con Co., Ltd* (unpublished manuscript).
- Keller, G. V., and Frischknecht, F. C., 1966, *Electrical methods in geophysical prospecting*: Pergamon Press, Inc.
- Kovacs, A., and Holladay, J. S., 1990, Sea-ice thickness measurements using a small airborne electromagnetic sounding system: *Geophysics*, **55**, 1327–1337.
- Kovacs, A., Holladay, J. S., and Bergeron, C. J., Jr., 1995, The footprint/altitude ratio for helicopter electromagnetic sounding of sea-ice thickness: Comparison of theoretical and field estimates: *Geophysics*, **60**, 374–380.
- Kovacs, A., and Morey, R. M., 1988, Electromagnetic measurements of a second year sea ice floe, in Sackinger, W. M., and Jeffries, M. O., Eds., *Port and ocean engineering under arctic conditions*: POAC, **1**, 121–136.
- 1991, Sounding sea-ice thickness using a portable electromagnetic induction instrument: *Geophysics*, **56**, 1992–1998.
- Kovacs, A., Valleau, N. C., and Holladay, J. C., 1987, Airborne electromagnetic sounding of sea-ice thickness and subice bathymetry: *Cold Regions Sci. and Tech.*, **14**, 289–311.
- Leppäranta, M., and Manninen, T., 1988, The brine and gas content of sea ice with attention to low salinities and high temperatures: Finnish Institute of Marine Research, Internal Report 2.
- Liu, G., and Becker, A., 1990, Two-dimensional mapping of sea-ice keels with airborne electromagnetics: *Geophysics*, **55**, 239–248.
- Liu, G., Kovacs, A., and Becker, A., 1991, Inversion of airborne electromagnetic survey data for sea-ice keel shape: *Geophysics*, **56**, 1986–1991.
- Maykut, G. A., 1986, The surface heat and mass balance, in Untersteiner, N., Ed., *The geophysics of sea ice*: Plenum, 395–463.
- Mitchell, J. F. B., Manabe, S., Meleshko, V., and Tokioka, T., 1990, Equilibrium climate change and its implications for the future, in Houghton, J. T., Jenkins, G. J., and Ephraums, J. J., Eds., *Climate change—the IPCC scientific assessment*: Cambridge Univ. Press, 131–172.
- Morey, R. M., Kovacs, A., and Cox, G. F. N., 1984, Electromagnetic properties of sea ice: *CRREL Monogr.*, **84**-2.
- Multala, J., Hautaniemi, H., Oksama, M., Leppäranta, M., Haapala, J., Herlevi, A., Riska, K., and Lensu, M., 1995, Airborne electromagnetic surveying of baltic sea ice: Report series in Geophysics, Univ. of Helsinki, Dept. of Geophysics, 31.
- Sinha, A. K., 1976, A field study for sea ice thickness determination by electromagnetic means: *Geol. Surv. of Canada, GSC Paper* 76-1C, 225–228.
- Stogryn, A., and Desargant, G. J., 1985, The dielectric properties of brine in sea ice at microwave frequencies: *IEEE Trans. on Antennas and Propagation*, **AP-33**, 523–532.
- Thyssen, F., Kohnen, H., Cowan, M. V., and Timco, G. W., 1974, DC resistivity measurements on the sea ice near Pond Inlet, N.W.T (Baffin Island): *Polarforschung*, **44**, 117–126.
- UNESCO, 1983, Algorithms for computation of fundamental properties of sea water: *Unesco Tech. Pap. in Mar. Sci.*, **44**.
- Wadhams, P., and Martin, S., 1990, Processes determining the bottom topography of multiyear Arctic sea ice, in Weeks, W. F., and Ackley, S. F., Eds., *Sea ice properties and processes*: *CRREL Monogr.* **90**-1, 136–141.
- Wadhams, P., Tucker III, W. B., Krabill, W. B., Swift, R. N., Comiso, J. C., and Davis, N. R., 1992, Relationship between sea ice freeboard and draft in the Arctic Basin, and implications for ice thickness monitoring: *J. Geophys. Res.*, **97**, 20,325–20,334.
- Ward, S. H., and Hohmann, G. W., 1988, Electromagnetic theory for geophysical applications, in Nabighian, M. N., Ed., *Electromagnetic methods in applied geophysics—theory*, volume 1: *Soc. Expl. Geophys. Monograph*, **3**, 131–313.